



# Evidence for a persistent magma reservoir with large melt content beneath an apparently extinct volcano

M. Laumonier<sup>a,\*</sup>, O. Karakas<sup>b</sup>, O. Bachmann<sup>b</sup>, F. Gaillard<sup>c</sup>, R. Lukács<sup>d</sup>, I. Seghedi<sup>e</sup>,  
T. Menand<sup>a</sup>, S. Harangi<sup>d,f</sup>

<sup>a</sup> Université Clermont Auvergne, CNRS, IRD, OPGC, Laboratoire Magmas et Volcans, F-63000 Clermont-Ferrand, France

<sup>b</sup> Department of Earth Sciences, Institute of Geochemistry and Petrology, ETH Zurich, Switzerland

<sup>c</sup> Université d'Orléans, CNRS, BRGM, ISTO, UMR 7327, F-45071, France

<sup>d</sup> MTA-ELTE Volcanology Research Group, Budapest, Hungary

<sup>e</sup> Institute of Geodynamics, Romanian Academy, Bucharest, Romania

<sup>f</sup> Eötvös Loránd University, Department of Petrology and Geochemistry, Budapest, Hungary

## ARTICLE INFO

### Article history:

Received 5 December 2018

Received in revised form 28 May 2019

Accepted 5 June 2019

Available online xxxx

Editor: J. Brodtholt

### Keywords:

seemingly inactive volcano

magma storage

numerical simulation

mush petrology

in-situ electrical-conductivity measurement

geophysical interpretation

## ABSTRACT

Most active volcanoes display eruption frequencies of 10–1000s years but a class of volcanic systems has extremely long repose-time (>10's kyr), and are deemed as extinct. Yet, some reawaken, posing a particular threat because little is known about the way they endure and stir back to life. Reawakening primarily depends on the nature of the subvolcanic magma reservoir, especially the presence and distribution of melt. Here, we integrate petrology, thermobarometry, thermomechanical models, geophysics and *in situ* electrical conductivity measurements to show that the magma storage beneath Ciomadul, a seemingly inactive volcano in eastern-central Europe that last erupted 30 ka, may still hold 20 to 58 km<sup>3</sup> of water-rich silicic melt, constituting up to 20–58% in parts of the upper crustal crystal mush body. Such a melt volume exceeds the volume of erupted lava over the entire history of the volcano. This illustrates the important longevity of a magmatic reservoir at temperature above the solidus, which implies that there is still a potential for rapid mush rejuvenation. That a seemingly dead volcano like Ciomadul is actually capable of erupting in the future calls for renewed attention to “inactive” volcanoes worldwide and perhaps for a redefinition of their activity/inactivity status.

© 2019 Elsevier B.V. All rights reserved.

## 1. Introduction

### 1.1. Magma storage beneath volcanoes

Magma reservoirs beneath volcanoes are considered to subsist dominantly at high crystallinity (Annen et al., 2006; Bachmann and Huber, 2016; Cashman et al., 2017) (“crystal mush”), surviving over 10's or 100's thousands of years (Bachmann, 2010; Cooper, 2015; Costa, 2008; Gelman et al., 2013) as they are episodically replenished by magma influx from below (Annen et al., 2006; Karakas et al., 2017). Within these bodies, melt-dominated (>~50% melt) regions, *i.e.* magma chambers, can form and feed volcanic activity. However, due to difficulties in detecting and probing such molten bodies at depth, the magma storage conditions are still debated based on three main hypotheses: reservoirs (1) contain a significant amount of melt for long periods of time

(Barboni et al., 2016), (2) remain dominantly just above the solidus at relatively low melt fraction, with some small melt-rich pockets periodically forming by extraction from the much larger surrounding mush zone (Cooper, 2019; Szymanowski et al., 2017) or (3) they are stored dominantly in subsolidus state (Cooper, 2019; Rubin et al., 2017). Existence and distribution of melt in the storage zone greatly affects the reactivation potential of a magma body (Huber et al., 2011) and defines the nature of a volcano, *i.e.* whether it is still potentially active or considered extinct. In this context, the prolonged preservation of significant melt fractions in the storage region has a particular importance, and its detection and description is crucial to assess the level of potential volcanic hazards.

Ciomadul, located in eastern-central Europe (Fig. 1) is an excellent example of a seemingly inactive volcano (Harangi et al., 2015a; Szakács et al., 2015), because its eruption chronology shows long quiescence periods (Molnár et al., 2018) between active phases, with its last eruption occurring around 30 ka (Harangi et al., 2015a; Karátson et al., 2016; Molnár et al., 2019). It consists of fairly homogeneous high-K dacites, but contains complexly

\* Corresponding author.

E-mail address: mickael.laumonier@gmail.com (M. Laumonier).

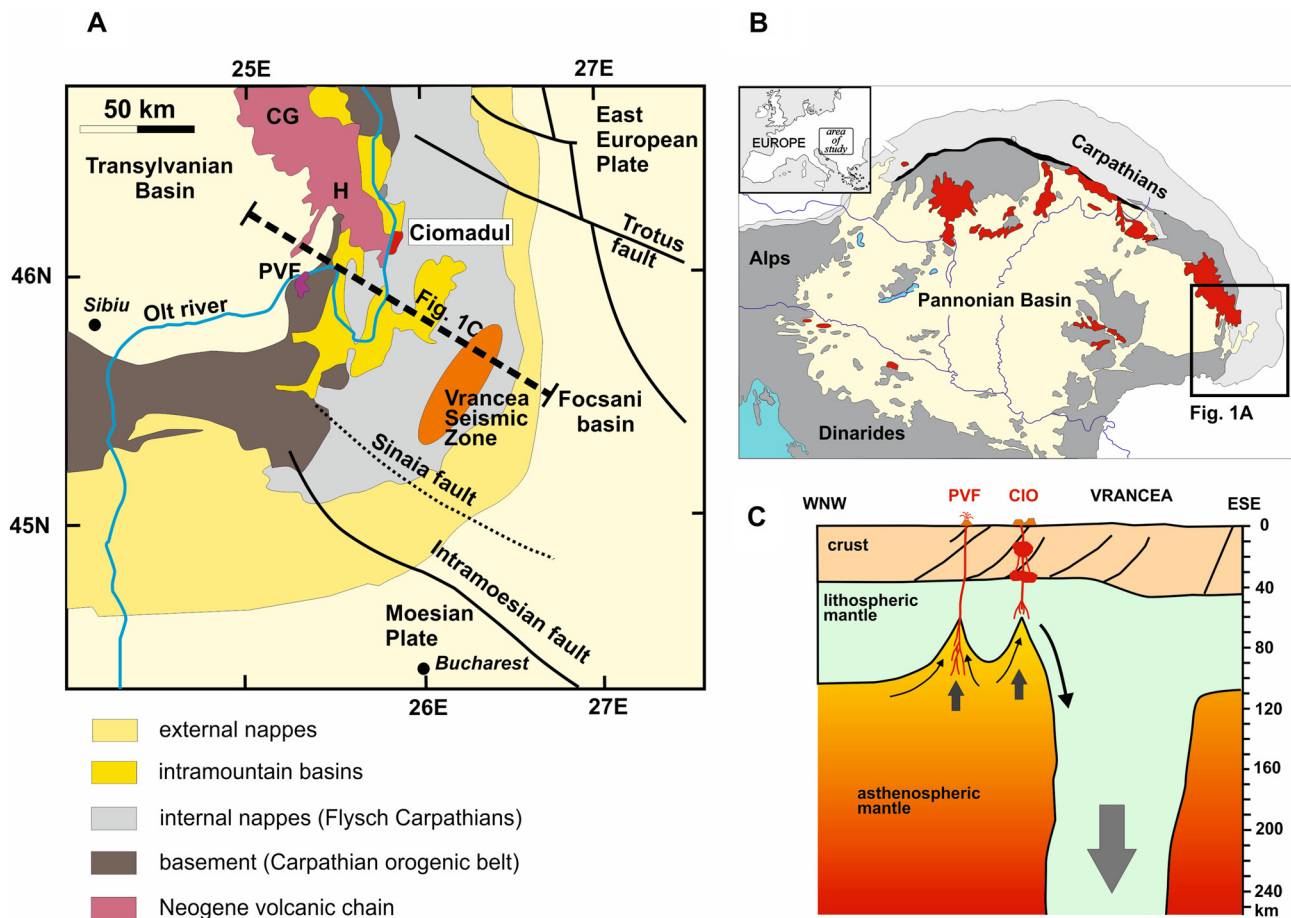


**Fig. 1.** Geological context of Ciomadul volcano. (A) Location of the Ciomadul volcanic complex in the southeastern Carpathian area of the Carpathian-Pannonian Region (simplified geological map after Cloetingh et al., 2004 and Martin et al., 2006). CG=Călimani-Gurghiu volcanic complex, H=Harghita volcanic complex, PVF = Perșani Volcanic Field. (B) The study area in Europe and in the Carpathian-Pannonian region with the surface exposures of the Miocene to Quaternary calc-alkaline andesitic to dacitic volcanic areas (red colour). (C) Cross section through the Quaternary volcanic areas and the Vrancea seismic zone showing conceptual model for lower lithospheric ruptures due to the downgoing vertical lithospheric slab beneath the Vrancea Zone (modified after Seghedi and Downes, 2011; PVF = Perșani Volcanic Field; CIO = Ciomadul Volcanic Complex). (For interpretation of the colours in the figure, the reader is referred to the web version of this article.)

zoned crystals of plagioclase, amphibole and biotite (Harangi et al., 2015b). Although Ciomadul has been in a seemingly inactive state for a long time, several lines of evidence support a long-lived system holding a potentially active magma storage (Harangi et al., 2015a, 2015b) (“PAMS” volcano): (1) significant CO<sub>2</sub>-emanations with strong magmatic component (Kis et al., 2019), (2) wide range of zircon crystallization ages (from 60 ka to 350 ka) suggestive of a long-lived system till today (Harangi et al., 2015a) and (3) petrological evidences for the presence of felsic crystal mush and open-system magmatic processes in the magma storage (Harangi et al., 2015b; Kiss et al., 2014). Furthermore, (4) geophysical anomalies such as low electrical resistivity and seismic wave attenuation were observed from the base of the crust and may reveal the subvolcanic plumbing system (Harangi et al., 2015b; Popa et al., 2012). The magnetotelluric survey evidenced a conductive body from about 5 to 27 km depth with a particularly high signal between 9 and 21 km depth (Harangi et al., 2015b) (electrical resistivity <2 ohm.m). Such anomaly is consistent with the existence of a magma reservoir in the middle to upper crust, but this shallow conductor makes it difficult to resolve potential underlying features (Bedrosian, 2007). From geophysics, it is thus uncertain whether there is a continuous mushy zone down to the lower crustal hot zone or not. The status of Ciomadul’s plumbing system, *i.e.* the existence and amount of melt, cannot be elucidated solely from geophysical observations; petrological data could also help to reveal the trans-crustal magmatic system (Cashman et al.,

2017) beneath Ciomadul, as it has been suggested for other magma storage systems around the world (Bachmann and Huber, 2016; Christopher et al., 2015).

In order to better constrain the current state of Ciomadul volcano, we propose a direct modelling of the geophysical signal of its plumbing system: a petrological analysis is used to build numerical simulations of the thermal evolution of the magmatic reservoir that is converted into electrical conductivity distribution. The integration of this modelling with geophysical observations indicates that a significant amount of water-rich silicic melt (at minima 15%) must still be present in the upper crust beneath the volcano, implying that the reservoir is likely to have been kept in warm enough conditions to preserve sizeable domains in near-eruptible state. This calls for attention about long-dormant volcanoes and questions the definition of potentially active, dormant and extinct volcanoes (Szakács, 1994), since their plumbing systems may be comparable to active volcanoes.

## 1.2. Geological settings of Ciomadul Volcano

Ciomadul is located at the southern edge of the ca. 160 km long Calimani-Gurghiu-Harghita volcanic chain, and represents the latest manifestation of the Neogene to Quaternary volcanism in the post-collisional tectonic setting of the Carpathian-Pannonian Region (Fig. 1) (Harangi and Lenkey, 2007; Seghedi and Downes, 2011). The volcanism of Ciomadul occurred in a geodynamically

**Table 1**

Bulk chemical composition (in wt%) of the Ciomadul dacite determined by ICP-MS method (Vinkler et al., 2007) and of the dry starting glass (30 analyses) after melting of the Ciomadul sample determined by Electronic MicroProbe Analysis (standard deviation in italic font).

	SiO <sub>2</sub>	TiO <sub>2</sub>	Al <sub>2</sub> O <sub>3</sub>	FeO	MnO	MgO	CaO	Na <sub>2</sub> O	K <sub>2</sub> O	P <sub>2</sub> O <sub>5</sub>	Total
Vinkler et al., 2007	65.41	0.36	16.93	2.75	0.05	2.32	4.26	4.58	3.15	0.18	99.99
Vinkler et al., 2007	65.19	0.36	16.99	2.72	0.06	2.39	4.07	4.74	3.3	0.17	99.99
This study	65.79	0.35	16.77	2.10	0.06	2.09	3.83	4.73	3.41	nd	99.12
	<i>0.35</i>	<i>0.05</i>	<i>0.18</i>	<i>0.10</i>	<i>0.04</i>	<i>0.09</i>	<i>0.08</i>	<i>0.14</i>	<i>0.11</i>	<i>nd</i>	<i>0.47</i>

still active region, close to the Vrancea area, where a near-vertical lithospheric slab descending in the upper mantle causes frequent deep-hypocentres (70–170 km) earthquakes (Ismail-Zadeh et al., 2012). The latest eruptions for the last 1 Myr (Molnár et al., 2018) formed a volcanic dome field consisting of small volume (<0.5 km<sup>3</sup>) lava domes and the massive Ciomadul volcanic complex (8–14 km<sup>3</sup>). The Ciomadul volcanic complex is the amalgamation of several lava domes truncated by two explosive craters developed from 160 ka to 30 ka (Harangi et al., 2015a; Karátson et al., 2016; Molnár et al., 2019; Szakács et al., 2015).

## 2. Samples and methods

### 2.1. Starting material

The pumiceous dacite studied experimentally to determine the electrical conductivity belongs to one of the youngest eruptions of the Ciomadul (30 ka; Bixad locality; (Harangi et al., 2015a, 2010; Vinkler et al., 2007)). It represents a hot block-and-ash flow deposit formed either by fountain collapse of a Vulcanian explosion event such as occurred at Soufriere Hills, Montserrat in 1997 or explosive destruction of a growing lava dome (Vinkler et al., 2007). The bulk composition is high-K dacite typical of other volcanic products of Ciomadul (Molnár et al., 2018; Vinkler et al., 2007) (Table 1); it has relatively high Na<sub>2</sub>O (>4.2 wt%) and K<sub>2</sub>O (>3 wt%) contents, whereas the trace element composition is characterized by abundance of Ba and Sr (both elements are above 1500 ppm), depletion of Y (<10 ppm) and heavy rare earth elements (Yb < 1 ppm; Lu < 0.15 ppm). The dacite has a vesiculated glassy groundmass with ca. 30 vol.% phenocrysts of plagioclase, amphibole and biotite (see additional information in Results section). In the dome rocks, crystal clots frequently occur; they are mostly felsic (plagioclase and amphiboles in addition to accessory minerals, while some of them contain also quartz, K-feldspar and Fe-Ti oxides) and most of them contain interstitial vesicular glass. Furthermore, the dome rocks usually contain high-Mg minerals, such as olivine, clinopyroxene and orthopyroxene, both as solitary crystals and crystal clots. Their high mg-numbers (>85) indicate origin from less differentiated basaltic magma (Kiss et al., 2014; Vinkler et al., 2007). The monotonous chemical and petrologic natures of the erupted dacites at Ciomadul and volcanic neighbours over the past 1 Myr (Molnár et al., 2018) suggest a rather uniform petrogenesis.

The chosen dacite sample as starting material (BX08 (Harangi et al., 2015b)) is regarded as representative of potential magma nowadays residing in the subvolcanic system for the following reasons: (i) the dacite is the dominant eruption product and it represents the latest eruption phase (Harangi et al., 2015a), (ii) it contains relatively low amount of phenocrysts (<30%), suggesting that its bulk composition is close to the last melt composition before extraction from the reservoir and eruption, (iii) it does not contain significant amount of felsic crystal clots representing the cold crystal mush nor high-Mg mafic minerals (olivine and pyroxene) that represent fragments of mafic recharge.

The natural sample was crushed and fused at 1450°C under atmospheric conditions for 3 hours twice to ensure chemical homogeneity (Table 1). The resulting glass was crushed again and

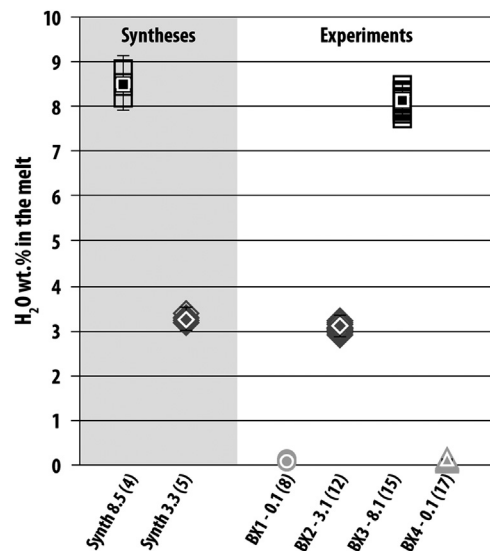


**Fig. 2.** Water content of dacitic glasses after hydration (Syntheses) and of experimental glasses after electrical conductivity measurements (“Experiments”). Empty symbols correspond to single analyses and full symbols to the average. The water variation before and after *in situ* electrical conductivity experiments is neglectable (lower than 5%).

used either to constitute the dry samples, or after hydration (with appropriate mass of water added) in piston cylinder to produce 3.1 and 8.1 wt.% water samples. Hydration syntheses were performed in welded shut gold palladium capsules at 1.5 GPa and 1300°C and held for 2 days to ensure a homogeneous water content.

The water concentration in synthetic glass and experimental products was measured by infra-red spectroscopy at ISTO (Microscope IR Continu μm coupled with a Nicolet 6700 spectrometer and a MCT detector, Orleans, France) using KBr beam splitter. Each measurement consisted of 128 scans with a resolution of 4 cm<sup>-1</sup>. The two hydrated syntheses and the post experimental glasses (dry and hydrous) were analyzed through 4 to 17 spots to check for homogeneity of the water concentration (Fig. 2). We calculated the water concentration using the Beer–Lambert law, with density and extinction coefficients from the literature (Ohlhorst et al., 2001), and the peak height absorbance corrected by a linear baseline. The thickness of the sample was measured by the calibrated stage of the microscope with an accuracy of less than 3 micrometers. To determine the water concentration of the water rich glasses (>8 wt.%), we used the molecular water (5200 cm<sup>-1</sup>) and OH- (4500 cm<sup>-1</sup>) stretching vibrations. The water content of “dry” glasses and glasses with ~3wt.% of water were measured using the fundamental H<sub>2</sub>O-stretching vibration (3530 cm<sup>-1</sup>). The propagated uncertainty results in a maximal error in [H<sub>2</sub>O] of 0.5 wt.% (Laumonier et al., 2017b).

### 2.2. Numerical simulation of the thermal evolution of Ciomadul upper reservoir

We used a two-dimensional thermal model modified from Karakas and Dufek (2015) and Karakas et al. (2017) and quantified

the magma evolution beneath Ciomadul volcanic system. The two-dimensional computational domain consists of a 60 km by 60 km section, where the upper 40 km represents the crust according to Hauser et al. (2007) and the remaining 20 km represents the upper mantle. Ciomadul volcanic system is idealized as having a 25 km upper-mid crust consisting of amphibolite facies metamorphic rocks and 15 km lower crust consisting of granulite facies metamorphic rocks. Initially, we assume that the crust has a steady-state geothermal gradient. The temperature profile is calculated using one-dimensional steady-state heat equation using radiogenic heating as a source term, where we assume that the radiogenic elements concentrate in the uppermost 12 km of the crust and decay exponentially with depth. We chose a temperature of 0°C for the surface, and a constant heat flux at the mantle-crust boundary. After calculation of the geothermal gradient, the side-boundary temperatures are kept constant during the transient calculations.

In order to quantify the magma evolution in the crust over time, we emplace dikes and sills incrementally over  $10^5$ – $10^6$  yr. Intrusion of magmas increases the temperatures of the surrounding crust, while the individual intrusions cool down due to heat transfer between the crust and the magma. We solve for transient heat conduction equation using latent heat as the source term. We follow the fully implicit finite volume scheme described by Patankar (1980) and use the iterative predictor-corrector algorithm of Voller and Swaminathan (1991). We assume that the magma emplacement process is stochastic and instantaneous as the dike emplacement timescales in nature (days to weeks) are much faster than the timescales that we consider in the model ( $10^5$ – $10^6$  yr). We acknowledge that the internal convection is important for the differentiation history of the crustal magma bodies (i.e. (Dufek and Bachmann, 2010; Petrelli et al., 2018)). However, over the time and length scales that we focus in the present study, we can neglect convection effects as conduction is the predominant process of heat transfer (Biot number ( $Bi$ )  $\ll 1$ ; (Carrigan, 1988)).

The latent heat evolution of the system during melting and crystallization is calculated using the phase diagrams of specific compositions from experiments and parameterized solutions from the rhyolite-MELTS thermodynamic software (Gualda et al., 2012). The melt fraction-temperature relationship of the metamorphic lithologies are taken from experiments of (Vielzeuf and Holloway, 1988). The intruded magma in the lower crust is assumed basaltic in composition (Nandedkar et al., 2014), and the intrusions in the upper crust are presumed dacitic (compiled from a number of measurements (Gelman et al., 2013)). We follow the two-stage process described in Karakas et al. (2017). The dikes and sills of basaltic composition are emplaced first in the lower crust over 1 Myr. Following this lower crustal magma emplacement, heat distribution in the crust is calculated and dacitic magma is then emplaced in the upper crust with intermediate to low fluxes ( $10^{-4}$  to  $10^{-3}$  km<sup>3</sup>/yr) for 500 kyr between 7 and 15 km depths, and assuming constant heat flux between the lower and upper crust. This allows us to calculate the thermal evolution as well as the melt evolution in the upper crust and to compare our results with the electrical conductivity, petrology, and magnetotelluric studies conducted in the Ciomadul Volcanic System.

### 2.3. *In situ* measurements of the electrical conductivity

Samples were cold pressed to form 5-mm diameter cylindrical pellets and drilled in the center leaving a 1-mm diameter hole. They were then inserted in a piston cylinder assembly modified for *in situ* electrical conductivity measurements (Laumonier et al., 2017b, 2015; Sifré et al., 2014): the sample is sandwiched by alumina disks to reduce the chemical contamination and surrounded by a platinum foil being the external electrode. The internal electrode is a 1-mm diameter platinum wire inserted in the sample

hole, in contact with the B-type thermocouple that was alternatively used to read the temperature right above the sample and to measure the sample resistance. Typical MgO, pyrex and talc were used to complete 3/4 or 1/2 inch assembly according to the desired pressure.

The sample electrical resistance was measured by an impedance gain phase analyzer Solartron and a 4-wire electrical set up adapted to the low resistance of hydrous silicate glasses. Resistance measurements were performed during heating and cooling paths, once the temperature was stable and with the thermocouple unplugged to avoid interferences with the electrical circuit. If the temperature differed by more than 5°C before and after the resistance measurement, it was repeated to reduce the uncertainty on the temperature. The electrical conductivity of the samples was calculated from their resistance and their geometry, resulting in a typical error smaller than 0.2 log unit in conductivity (S/m) (Laumonier et al., 2015). The retrieved electrical conductivity is a property of the melt being size-independent and that can directly be compared to the geophysical estimations of electrical conductivity in the crust beneath Ciomadul volcano.

## 3. Results

### 3.1. Petrology of the Ciomadul dacite

Mineral-scale petrological studies of the erupted products of Ciomadul provide constraints on the storage conditions prior to the latest eruption. Within the phenocryst assemblage, plagioclase and amphibole are the dominant minerals and occur in similar relative amounts.

Two generations of compositionally homogeneous plagioclase are present in the youngest dacite: (i) phenocryst-sized plagioclase with a spongy to sieved texture and occasional thin rim overgrowth of clear plagioclase; (ii) microphenocryst-sized plagioclase without resorption feature and a clear inner structure. In spite of the textural difference, both plagioclase phases have similar, relatively homogeneous chemical compositions ( $An = 40$ – $50$  mol% and  $FeO = 0.2$ – $0.3$  wt%). Intergrowth of both types of plagioclases with amphibole is fairly common. Amphiboles show various zoning patterns and cover a wide compositional range (Appendix A) that distinguishes three groups: low Al-Mg ( $Al^{IV} < 1.4$ , i.e.  $Al_2O_3 < 10$  wt%;  $MgO < 14$  wt%) hornblende, high Al-Mg ( $Al^{IV} > 1.4$ , i.e.  $Al_2O_3 > 10$  wt%;  $MgO > 16$  wt%) pargasite/Mg-hastingsite and an intermediate group ( $Al^{IV} > 1.4$ , i.e.  $Al_2O_3 > 10$  wt%;  $MgO = 13$ – $16$  wt%) (Fig. 3). Noteworthy, the intermediate composition amphibole occurs always at the outer zone of the phenocrysts and appears to be in equilibrium with the erupted melt. They are also found in amphibole crystal clots with interstitial glass.

### 3.2. Thermobarometry

Pressure and temperature of the magma storage can be determined using the amphibole and plagioclase compositions (Anderson et al., 2008; Holland and Blundy, 1994) on coexisting mineral pairs or using single amphibole compositions (Féménias et al., 2006; Mutch et al., 2016; Ridolfi et al., 2010; Ridolfi and Renzulli, 2012). However, the accuracy of these thermobarometric results is heavily debated in the literature: Kiss et al. (2014) and Erdmann et al. (2014) suggested that the barometric calculations introduced by Ridolfi et al. (2010) and Ridolfi and Renzulli (2012) may give often erroneous result. Furthermore, the amphibole thermometer (Ridolfi et al., 2010; Ridolfi and Renzulli, 2012) often yields higher temperature than that of Holland and Blundy (1994).

Gorini et al. (2018) recommended special cares when using the Ridolfi and Renzulli's thermobarometer (Ridolfi and Renzulli, 2012),



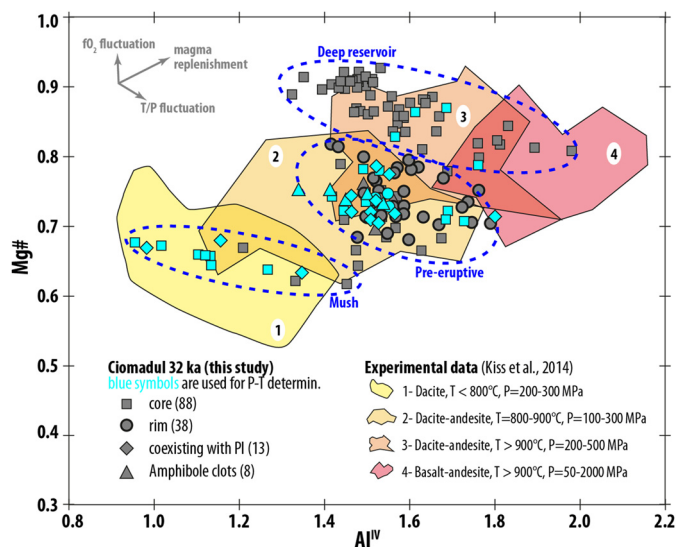


**Fig. 3.** Three compositional amphibole populations distinguished in the youngest dacite used in this study (symbols distinguish crystal cores and rims as well as amphiboles coexisting with plagioclase; numbers of analysis are indicated in parenthesis): low temperature and pressure (“mush”), high-temperature and high-pressure crystallization conditions (“deep reservoir”) and, noteworthy, amphibole rim always falling into the intermediate-temperature amphibole group (“pre-eruptive conditions”). P-T conditions from phase equilibrium experiments (yellow to red fields) are shown as compiled by Kiss et al. (2014).

which were followed here (Appendix A). As a result, less than 15% of the amphibole compositions with  $\text{Al}_2\text{O}_3 > 10$  wt% from the studied dacite sample passed the criteria and were acceptable for thermobarometric calculation (Appendix A). The pressure determination is also discussed with care due to the additional effect of melt composition on the amphibole chemistry (Erdmann et al., 2014; Kiss et al., 2014) (Fig. 3). For the low-Al ( $\text{Al}_2\text{O}_3 < 8$  wt%) amphiboles, we used the geobarometry as proposed by Mutch et al. (2016) along with the thermometer of Holland and Blundy (1994). Such amphiboles are often coexistent with plagioclase, K-feldspar, quartz, biotite, apatite and Fe-Ti oxides in the dome rocks (Kiss et al., 2014), a requisite for application of this barometry. On the other hand, the Ridolfi and Renzulli (2012)’s thermobarometric calculation was used with the modification as suggested by Gorini et al. (2018) for the high-Al ( $\text{Al}_2\text{O}_3 > 10$  wt%) amphiboles.

Based on the methodology described above, we obtained temperatures above 900°C and pressure from 230 to 420 MPa for the high-Al amphiboles. The low-Al amphiboles yield temperature between 720°C and 780°C and a pressure between 210 and 280 MPa. Noteworthy, we obtained a lower temperature of  $715 \pm 20^\circ\text{C}$  using low-Al amphibole and plagioclase pair thermometry (Holland and Blundy, 1994) for felsic clots found in lava dome rocks (Kiss et al., 2014). This is consistent with a crystal mush condition with more evolved melt (represented by interstitial glasses in felsic crystal clots and glass inclusions in plagioclase phenocrysts) residing at near-solidus, low-temperature environment (Appendix B). The intermediate amphiboles could have crystallized at similar pressure as the low-Al amphiboles, but at higher temperature (and from a slightly more mafic melt); plagioclase coexisting with intermediate-Al amphibole and Fe-Ti oxide thermometry (Appendix C) provide crystallization temperature of  $815 \pm 20^\circ\text{C}$ . We note that despite large uncertainties in the accuracy of most of these thermobarometers, this is a conservative estimate. We use the temperature conditions of the low Al and intermediate amphibole populations (715 and  $815^\circ\text{C}$  respectively) to determine the water content in the melt at depth.

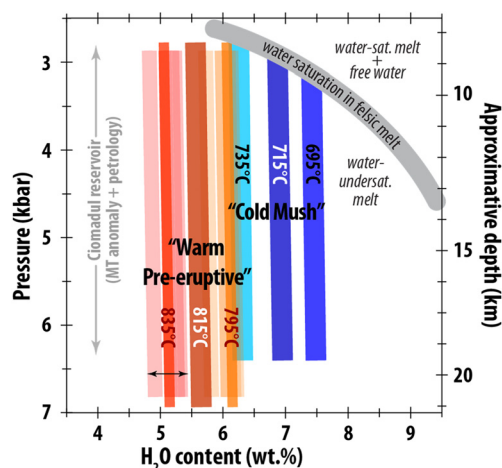


**Fig. 4.** Water concentration dissolved in the melt vs. pressure estimated by the plagioclase-liquid hygrometer of Waters and Lange (2015) for the “warm” and “cold” scenarios using amphibole glass inclusion and interstitial glass in amphibole clots, and the average glass composition from felsic clots, groundmass and glass inclusions in plagioclase respectively (Appendix B and E). The depth of Ciomadul potential magma reservoir determined from MT observation and petrological constraints is also reported, as well as the water saturation pressure in dacitic melt (Proureau and Scaillet, 2003). Among variable parameters, the temperature is the most influential on the water content as shown by the thick curves with labeled temperature. Propagation of uncertainties in water content due to minor variations in anorthite content (An40 to An50) and melt composition is revealed by half-transparent curves and the double arrow.

### 3.3. Determination of water concentration

Using the pre-eruption thermobarometric results, the water content of the melt was estimated using the plagioclase-liquid hygrometer as calibrated by Waters and Lange (2015). Plagioclase phenocrysts have fairly homogeneous composition in the studied Ciomadul dacite (An = 40–50 mol%; Appendix D), irrespective of their textural occurrence. Such variation in plagioclase composition has a poor effect on the water content calculation ( $\pm 0.1$  wt.%; Table 2). Similarly, the pressure variation determined from petrological data (200 to 500 MPa) has a direct effect on the water saturation but no significant influence on the calculated water content ( $\pm 0.1$  wt.%; Table 2), whereas the temperature affects it by  $\pm 0.5$  wt.%. (Table 2; Fig. 4; Appendix E). Plagioclase coexisting with intermediate-Al amphibole crystallized prior to eruption under relatively elevated storage temperature ( $815 \pm 20^\circ\text{C}$ ) yields melt water contents ranging from about 4.7 to 6.3 wt% assuming melt composition represented by the interstitial glass in amphibole clot and amphibole glass inclusions. (Table 2; Fig. 4; Appendix E). At low temperature (i.e.,  $\sim 715 \pm 20^\circ\text{C}$ ), the crystallization of An<sub>40–50</sub> plagioclase requires water content between 7.7 and 9.0 wt.%, when using the same melt composition (Appendix A and E). However, for such near-solidus, low-temperature condition, we anticipate a more evolved melt such as shown by interstitial glasses in felsic crystal clots of the lava dome rocks, groundmass and glass inclusions in plagioclase from the pumiceous dacite. Using the composition of the interstitial glass in felsic crystal clots, representative of a felsic mush, we deduce a conservative melt water content ranging between 6.0 and 7.7 wt% (Table 2; Fig. 4; Appendix A and E).

### 3.4. Thermal evolution of melt-bearing bodies beneath Ciomadul

Our numerical results are shown in Fig. 5. The evolution of the amount of magma through time is presented from the initiation of intrusions in the upper crust, 500 kyr ago, to 300 kyr in the future (Fig. 5A); numerical simulations show that existence of magma with high melt fraction (over 50%) is unlikely. However,

**Table 2**  
Conservative determination of the melt fraction in Ciomadul magmatic reservoir.

Parameter:	Temperature T	Pressure P	XAn in Plag	melt compo (wt.% SiO <sub>2</sub> )	XH <sub>2</sub> O in melt (wt.%)	Melt EC (Log scale)	Melt fraction
Methods:	Amphibole + Fe-Ti oxyde thermobarometry	thermo-barometry + geophysics	Microprobe analysis	Microprobe analysis	Plag-liq hygrometer	in situ exp.	Petrology + EC + geophysics**
<b>COLD preferred values</b>	<b>715°C</b>	<b>400 Mpa</b>	<b>0.45</b>	<b>74.5</b>	<b>7.0</b>	<b>-0.04</b>	<b>0.42 +/- 0.05</b>
T-XH <sub>2</sub> O trade-off	+/- 20°C				6.4 – 7.4	-0.21 to 0.09	0.28 – 0.54
P-XH <sub>2</sub> O trade-off		250 – 500 Mpa			6.9 – 7.0	-0.08 to -0.01	0.35 – 0.48
XAn-XH <sub>2</sub> O trade-off			0.40 – 0.50		6.9 – 7.0	-0.06 to -0.04	0.37 – 0.47
Melt compo-XH <sub>2</sub> O trade-off				73.3 – 75.9	6.8 – 7.2	-0.08 to -0.01	0.34 – 0.49
Cumulated uncertainties	+/- 20°C	250 – 500 Mpa	0.40 – 0.50	73.3 – 75.9	6.0 – 7.7	-0.30 to 0.17	0.25 – 0.58
<b>WARM preferred values</b>	<b>815°C</b>	<b>400 Mpa</b>	<b>0.45</b>	<b>69.9</b>	<b>5.6</b>	<b>0.02</b>	<b>0.35 +/- 0.04</b>
T-XH <sub>2</sub> O trade-off	+/- 20°C				5.1 – 6.1	-0.12 to 0.16	0.24 – 0.51
P-XH <sub>2</sub> O trade-off		250 – 500 Mpa			5.5 – 5.6	-0.01 to 0.05	0.30 – 0.43
XAn-XH <sub>2</sub> O trade-off			0.40 – 0.50		5.5 – 5.6	0.01 to 0.02	0.32 – 0.41
Melt compo-XH <sub>2</sub> O trade-off				68.6 – 71.0	5.3 – 5.7	-0.03 to 0.04	0.31 – 0.44
Cumulated uncertainties	+/- 20°C	250 – 500 Mpa	0.40 – 0.50	68.6 – 71.0	4.7 – 6.3	-0.16 to 0.22	0.20 – 0.53

The “preferred values” are taken from the mean of the range of each parameter while the “cumulated uncertainties” correspond to the conservative water concentration and melt fraction estimations by cumulating uncertainties.

\* Melt composition from natural sample to assess the water content with hygrometer of Waters and Lange (2015). In the Table is presented SiO<sub>2</sub> variation only.

\*\* Considering the uncertainty +/- 0.05 log unit on the electrical anomaly and using melt composition of the Ciomadul dacite. Abbrev.: Xan: Anorthite content in plagioclase; melt compo: chemical composition of the melt used in the hygrometer model; XH<sub>2</sub>O: water concentration obtained by hygrometer of Waters and Lange (2015) EC: electrical conductivity.

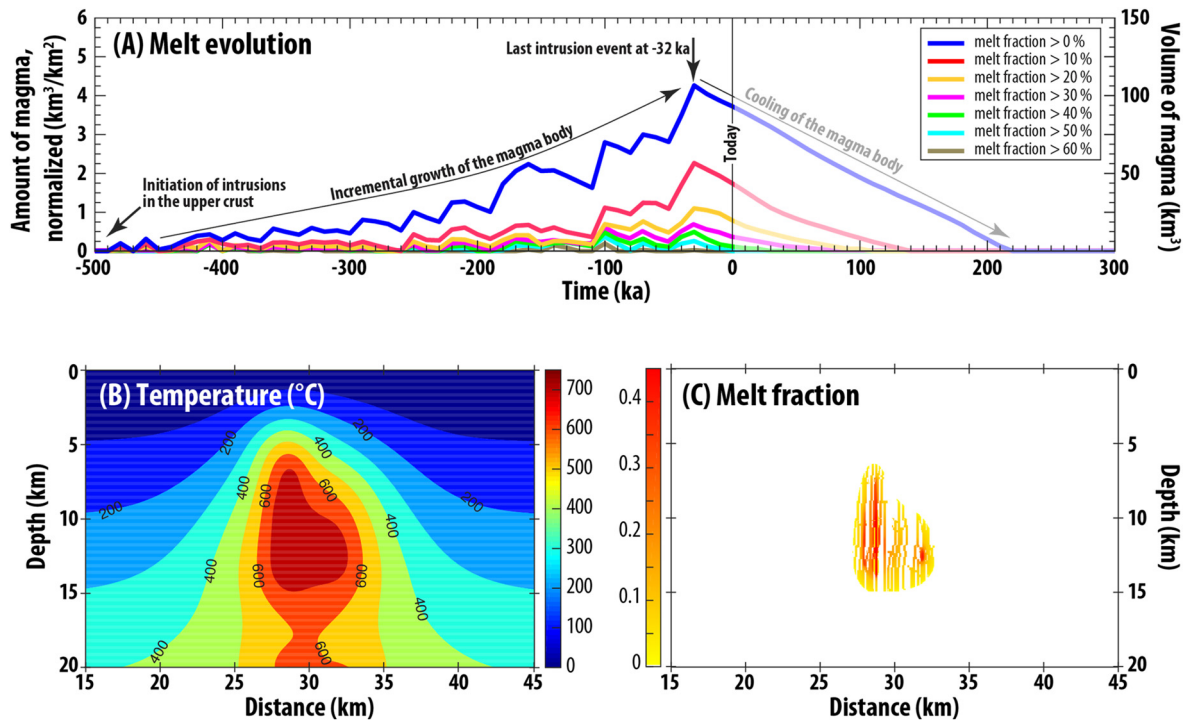


**Fig. 5.** Melt and temperature in the upper crustal magma system. (A) The upper crustal magma body grows with incremental and stochastic intrusions of magma over 470 kyr, until the last 32 ka eruption of Ciomadul. The cooling timescale is simulated by stopping magma emplacement at 470 kyr (marked as “last intrusion event”) and quantifying the volume of magma in the reservoir over time until the entire system reaches solidus. Each broken lines shows the predicted volume of magma with a certain melt fraction indicated in legend. For instance, today, numerical simulations predict about 100 km<sup>3</sup> of magma above the solidus (melt fraction > 0), and about 20 km<sup>3</sup> of magma with more than 20% of melt. (B) Temperature profile after 500 kyr (today) in the upper magma body from numerical simulation. (C) Current melt fraction distribution from numerical simulation.

magma with 10 to 30% of melt may be relatively abundant, from about 16 to 40 km<sup>3</sup>. The calculated thermal state of the upper crustal magma storage is consistent with petrological results and thermal calculations show that current temperature at the centre of the mush body still reaches 700–750°C, allowing, locally, melt fractions up to 40% (Fig. 5B & C). These local high melt fractions do not concentrate but are instead discretely distributed (Fig. 5C).

In order to quantify the cooling timescale of the magma body, we simulated the system until it cools down below its solidus

under two cases. The first one implies intrusions from –500 to –32 kyr (Fig. 5A). To compare, the second case simulate intrusion from –500 to 0 kyr (i.e. till today). In both cases, where we simulated different conditions (continuous intrusions vs. no intrusions) over the last 30 kyr, we do not observe significant differences in the temperature profile, the cooling timescale or in the average melt fraction of the magma body because latent-heat buffering at high crystallinity (near-eutectic conditions) maintain the system above the solidus for extended periods of time (Huber et al., 2009).

**Table 3**

Sum up of experimental conditions: duration, water content and pressure of each run as well as the temperature range used for the determination of the activation energy and pre exponential factor based on equation (1).

Exp #	Duration (h:mm)	H <sub>2</sub> O (wt.%)	Pressure (GPa)	Temperature range (°C)	Activation energy (J)	Preexponential factor (S/m)
BX08-1	1:05	0.1	0.7	281	65807	164
BX08-2	1:51	3.1	1.3	230	66815	526
		3.1	0.7	280	67617	491
BX08-3	2:13	8.1	2.8	178	76417	3639
		8.1	1.1	130	66198	3021
BX08-4	0:55	0.1	2.9	247	79228	347

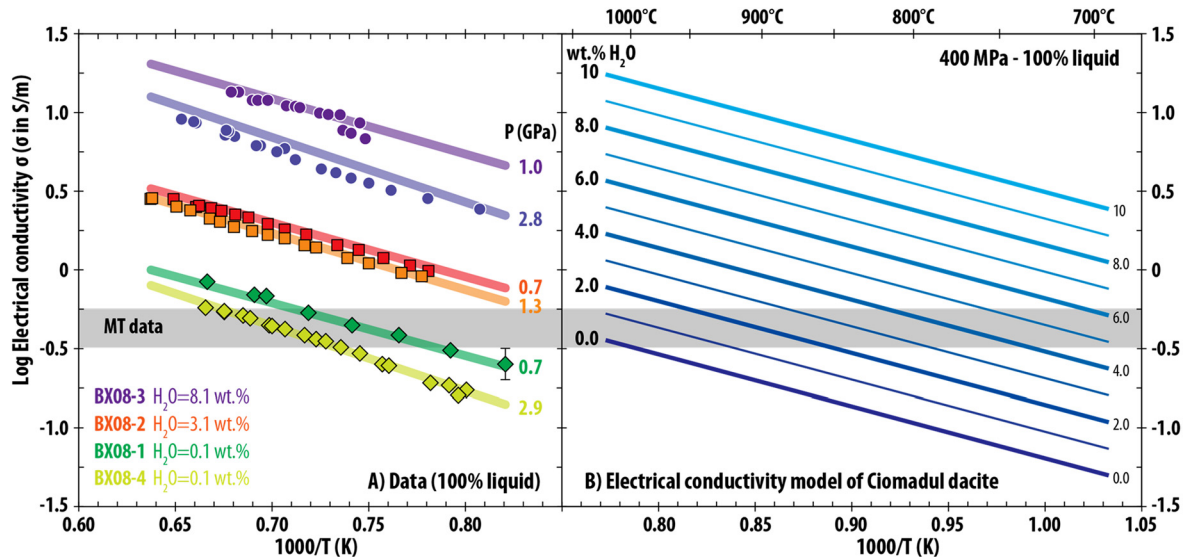


**Fig. 6.** Electrical conductivity data and model of the Ciomadul dacitic liquid. (A) Reciprocal temperature vs. electrical conductivity (log scale) of the Ciomadul dacite at different water contents and pressures. Symbols are the experimental data and compared with the general model calculated for the same conditions as each data set. The grey area labeled “MT data” corresponds to the geophysical electrical conductivity anomaly identified by (Harangi et al., 2015b). (B) Effect of water content, at a constant pressure of 400 MPa, on electrical conductivity of the Ciomadul dacite liquid as a function of the reciprocal temperature.

### 3.5. Laboratory-based determination of the dacite electrical conductivity

To verify the relevance of the thermal evolution of Ciomadul’s magmatic system determined by model calculation, we measured *in situ* the electrical conductivity of the dacite from the 32 ka Ciomadul eruption that we compare with the magnetotelluric observations of Ciomadul’s underground (Harangi et al., 2015b). Run conditions include pressures from 0.7 to 2.9 GPa, water contents from 0 to 8.1 wt.% and temperatures up to 1300°C, largely covering conditions encountered in the crust (Table 3). The results show a positive correlation of the electrical conductivity with temperature and water content, and a negative correlation with pressure typical of intermediate to felsic silicate melts (Fig. 6A). Contrary to the results found on the low Na-content (2.1 wt.%) dacite from Uturuncu volcano (Laumonier et al., 2015), both activation energy and volume activation are constant here, and the effect of water on the electrical conductivity essentially reflects the evolution of the Arrhenius pre-exponential factor. The remaining variable affecting the electrical conductivity imaged by geophysical surveys is thus the melt fraction ( $\Phi_m$ ), which is discussed below (section 4.3).

## 4. Discussion

### 4.1. Magma storage conditions beneath Ciomadul

Fig. 7 shows the interpretative anatomy of the Ciomadul plumbing systems based on the petrology of the erupted products. The high-Al and high-Mg-pargasitic amphiboles are inferred to derive

from a relatively deep (300–550 MPa, *i.e.* 10–18 km depth) part of the upper crustal magma storage at relatively high temperature (>900°C; Fig. 3 & 7), and were transported to the shallow depth during recharge events. There are no quantitative petrologic constraints about deeper crystallization conditions, *i.e.*, above 550 MPa, although occurrence of Mg-rich minerals and crystal clots involving olivine, clinopyroxene and orthopyroxene in the dome rocks suggests that less differentiated basaltic magmas are also involved in the magma genesis (Kiss et al., 2014; Vinkler et al., 2007). Such primitive phase assemblages could mirror magmatic processes at the crust-mantle boundary or in the lower crust, akin to the MASH Zone of Hildreth and Moorbath (1988) or to the hot zone of Annen et al. (2006).

The low-Al amphiboles (hornblendes) and plagioclases imply a relatively shallow (<300 MPa pressure/5–9 km depth), low-temperature (700–760°C) silicic mushy magma storage. The low temperature conditions calculated from amphibole and plagioclase pairs are supported also by the zircon and titanite temperature results, which give range from 660 to 730°C (using  $a_{\text{TiO}_2} = 0.6$  and  $a_{\text{SiO}_2} = 1$  and the thermometers of Ferry and Watson (2007) and Watson et al. (2006), respectively). Fragments of this near-solidus felsic crystal mush are represented by crystal clots with interstitial evolved glass composition in the dome rocks.

The intermediate group of amphibole accompanied with plagioclase reveals similar depth as the low-temperature hornblendes, but has higher crystallization temperature (815°C  $\pm$  20). Textural evidences suggest that this could represent conditions prior to the last eruption of Ciomadul. Texture and the temperature of the Fe-Ti oxides imply that they could have re-equilibrated with



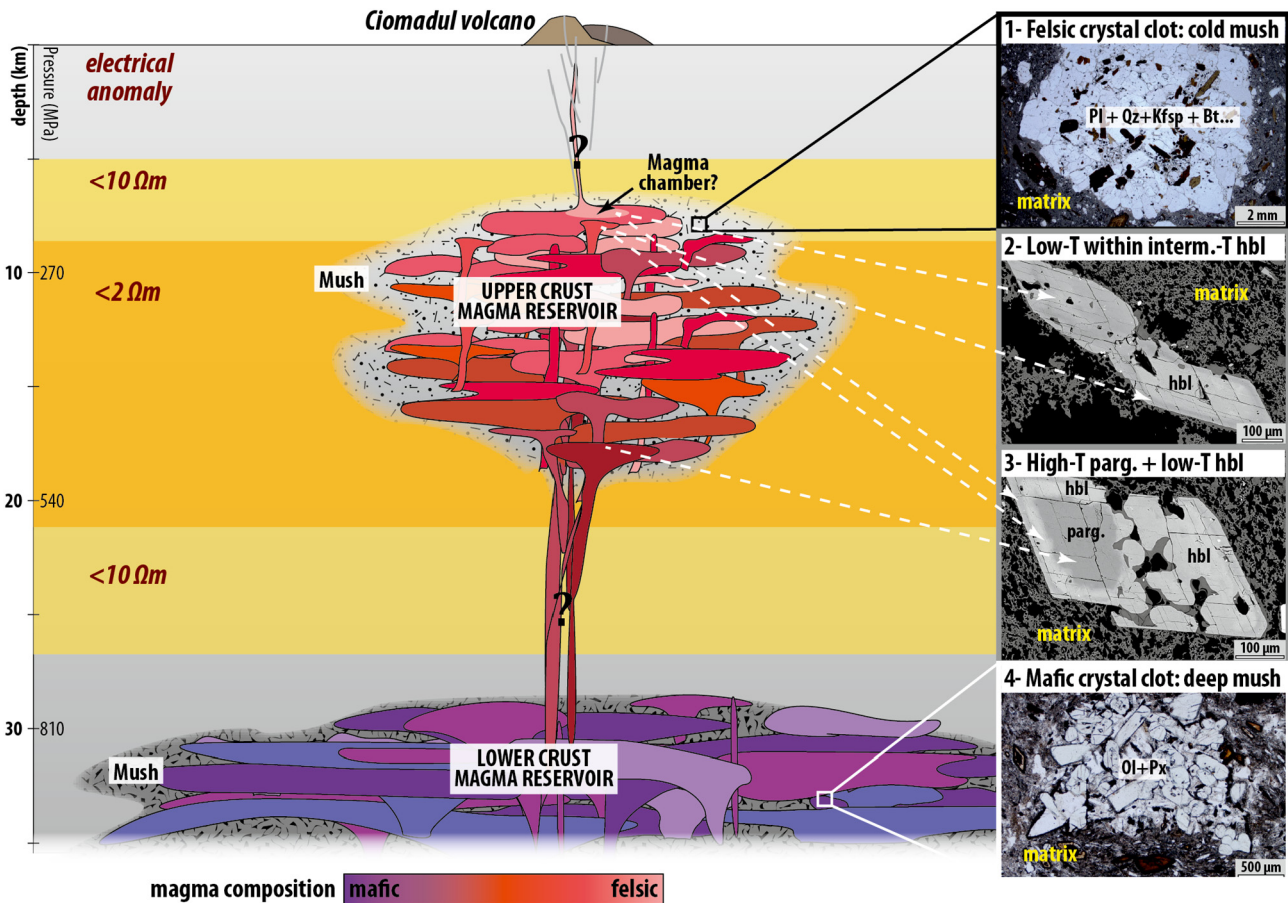


**Fig. 7.** Petrological and magnetotelluric inference for the transcrustal magma plumbing system beneath Ciomadul. The presence for a lower crustal mafic magma storage is demonstrated by mafic crystal clots (4) found in erupted products consisting of high-Mg olivine (Ol) and clinopyroxene (Px) and low resistivity anomaly at the periphery of the upper crustal magma reservoir (see Fig. 8c in (Harangi et al., 2015b)). Such mafic magmas differentiate and yield evolved magmas that rise through the crust, and cool down to build up an upper crustal felsic magma reservoir. At this stage, it is uncertain whether there is a continuous mushy magma storage between the lower and upper reservoirs. Locally, the upper magma reservoir could contain relatively high melt fraction resulting in potential magma chambers that feed volcanic eruptions. The cold mush state in the upper crustal reservoir is represented by felsic crystal clots (1) made of plagioclase (Pl), quartz (Qz), K-feldspar (Kfsp), biotite (Bt) and accessory minerals as well as amphiboles (hornblende) consistent with a temperature slightly above the solidus. Complex amphibole textures (2 and 3) indicate crystallization at different temperature and pressure and mixing of magma batches with distinct compositions suggesting a polybaric structure of the magma reservoir. The electrical anomaly identified by geophysical investigations is consistent with petrological deductions for the upper crustal reservoir (Harangi et al., 2015b).

the low-T melt and their compositions preserved during the rapid magma ascent. Such features suggest that within the felsic mush body, melt-rich zones with higher temperature existed, presumably after recharge events potentially leading to the development of eruptible magma pockets.

In summary, we infer a vertically extended (from ~5 km to ~18 km) felsic magma storage underlain by a hot zone of mafic magma accumulation from the crust-mantle boundary (~40 km) up to ~30 km depth (Fig. 7). Mafic minerals such as olivines, clinopyroxenes and orthopyroxenes with high Mg-numbers ( $>0.85$ ) call for the role of mafic recharge originating from deeper in the system (Fig. 7). However, we lack so far of evidence that would constrain the connection of a potential lower crustal mafic reservoir with the upper one (the latter being responsible for the observed electrical conductivity anomaly). Magma batches from this root zone ascend to the upper part of the magma storage and occasionally mix with the more evolved magmas. These fresh magmas locally heated and partially melted the crystal assemblage and transported high-Al amphiboles (pargasites/Mg-hastingsites) formed at higher temperature ( $>900^\circ\text{C}$ ) and at greater depth into the shallow felsic crystal mush zone. Following magma recharge, the magma condition stabilized at  $\sim 800^\circ\text{C}$ , where the rims of the amphiboles were formed and the Fe-Ti oxides re-equilibrated. This implies that before the latest eruption,

the magma storage was thermally heterogeneous, comprising both low- and intermediate temperature zones that fed the eruption, as well as deeper high-temperature zones. The upper part of the felsic crystal mush zone could have resided at relatively low temperature ( $<750^\circ\text{C}$ ) for a prolonged ( $\gg 100$  ka) period as shown by U-Th dates of zircons (Harangi et al., 2015a). The depth range of the felsic upper crustal magma storage is consistent with the magnetotelluric low-resistivity anomaly (Harangi et al., 2015b). Based on the monotonous chemical and petrologic natures of Ciomadul dacites over the past 1 Myr (Molnár et al., 2018, 2019), one can expect similar storage conditions over time.

#### 4.2. Definition of an electrical conductivity model for the Ciomadul dacite

The electrical conductivity of the dacite melt follows the Arrhenius law:

$$\sigma_{\text{dacite}} = \sigma_0 \cdot \exp^{-(E_a + P\Delta V)/RT} \quad (1)$$

where  $\sigma_0$  is a pre exponential factor ( $\text{S}\cdot\text{m}^{-1}$ ),  $E_a$  the activation energy (J),  $P$  the pressure (bar),  $\Delta V$  the activation volume ( $\text{cm}^3\cdot\text{mol}^{-1}$ ),  $R$  the gas constant and  $T$  the temperature (K).  $\sigma_0$  can be modelled by 4 parameters  $a$  to  $d$  in the equation established by Laumonier et al. (Laumonier et al., 2017b, 2015):



$$\sigma_0 = \exp\{(aw + b) + P * (cw + d)\} \quad (2)$$

where  $w$  is the water concentration in wt.% and  $P$  is the pressure in bars. The fitting parameters are  $a = 0.395 \pm 0.077$ ;  $b = 4.65 \pm 0.26$ ;  $c = -1.77E - 06 \pm 3.04E - 07$  and  $d = 3.91E - 05 \pm 1.24E - 05$ . Contrary to previous empirical model determined for intermediate magmas from Cerro Uturuncu (Laumonier et al., 2017b, 2015), activation energy and the activation volume were found to be constant here ( $Ea = 60,000 \pm 3,000 \text{ J.mol}^{-1}$ ;  $\Delta V = 6.54 \pm 1.41 \text{ cm}^3.\text{mol}^{-1}$ ). The fitted values  $a$  to  $d$ ,  $Ea$  and  $\Delta V$  returned a correlation coefficient of 0.99. The effect of temperature and water content is illustrated at 400 MPa in Fig. 6B.

Under dry conditions, the activation energy of the Ciomadul dacitic melt (60 kJ) is lower than the one of Uturuncu dacite (88 kJ), and better resembles the one of felsic compositions that contain similar sodium content (e.g. rhyodacite (Tyburczy and Waff, 1985) with  $Ea = 59 \text{ kJ}$ ; or a rhyolite (Gaillard, 2004)  $Ea = 65 \text{ kJ}$ ; Fig. 8). Based on the existent literature, the conductivity of dry intermediate to felsic melts varies over 2 orders of magnitude whereas it extends over 0.5 log unit under hydrous conditions (at 800°C, Fig. 8A). It positively correlates with temperature and water content, and negatively with pressure as other intermediate to felsic silicate melts (Chen et al., 2018; Gaillard, 2004; Guo et al., 2016; Laumonier et al., 2017b, 2015; Pommier et al., 2008; Tyburczy and Waff, 1985) (Fig. 8). Plotted against the sodium content, the electrical conductivity of felsic dry melts scatters while the one of hydrous melts defines a positive trend with increasing sodium content (Fig. 8B). In other words, the electrical conductivity of hydrous melts corresponding to a large number of magma reservoirs in the upper to middle crust (100 and 500 MPa) strongly depends on the sodium content. Therefore, we agree with the previous works concluding that sodium is the main charge carrier and the key controller of the electrical behaviour of dacitic and felsic melts in general (Chen et al., 2018; Gaillard, 2004; Gaillard and Marziano, 2005; Guo et al., 2016; Laumonier et al., 2015; Pommier et al., 2008).

#### 4.3. Determination of the melt fraction beneath Ciomadul

The numerical results predict the likely persistence of significant amounts of melt (up to ~40 %) locally under the Ciomadul volcano and a cooling timescale of the present-day Ciomadul reservoir of ~250 kyr (Fig. 5), a relatively long timescale even for a magmatic system of limited size. Such prediction are confronted to the melt fraction determined from geophysical observations and the electrical model: for both the relatively low-temperature crystal mush and warmer magma chamber conditions, we calculated the melt fraction – water content pairs that solve the electrical conductivity anomaly identified beneath Ciomadul volcano (Harangi et al., 2015b) ( $\text{Log } \sigma = -0.45$ ). The melt fraction of the magma was calculated using the modified Archie's law (Glover et al., 2000) with the electrical conductivity of the dacite determined here as conductive phase and the value  $0.001 \text{ S.m}^{-1}$  as the solid, resistive phase, corresponding to plagioclase, amphiboles or pyroxene crystals (Maury, 1968) or warm silicate rocks (Hashim et al., 2013). The exponent  $m = 1.05$  in the modified Archie's law was taken after Gaillard & Iacono-Marziano (Gaillard and Marziano, 2005). Due to the relatively large amount of melt (more than few percents), the conductivity of the solid phase has no significant effect, the liquid conductivity being the determinant one (Laumonier et al., 2017a).

We find that the melt fraction ranges from ~0.20 to 0.58 (Fig. 9A). In detail, the melt fraction inferred for both warm ( $0.35 \pm 0.04$ ) and cold ( $0.42 \pm 0.05$ ) scenarios explain the geophysical observations (Table 2), highlighting the primary effect of water on the electrical conductivity of such a magmatic system; both

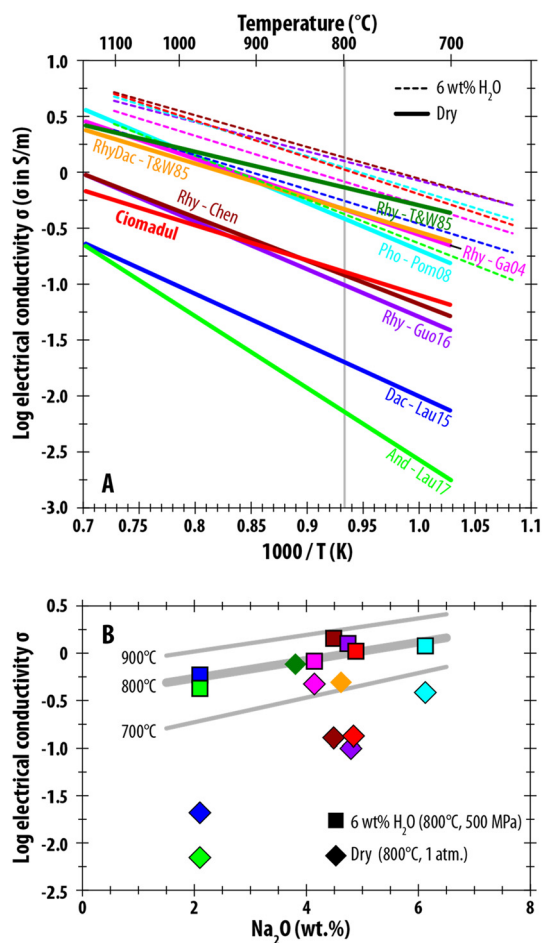


**Fig. 8.** Comparison of calculated electrical conductivity of Ciomadul dacite with data from literature. (A) Electrical conductivity (log scale) is plotted according to the reciprocal temperature of dry ( $P = 1 \text{ atm}$ ) and hydrous ( $P = 500 \text{ MPa}$ ) intermediate to felsic melts. Hydrous melts (dotted lines) and dry melts (continuous lines) respect the same color code (Chen et al., 2018; Gaillard, 2004; Guo et al., 2016; Laumonier et al., 2017b, 2015; Pommier et al., 2008; Tyburczy and Waff, 1985). (B) Electrical conductivity (log scale) at 800°C (symbols and thick curve) as a function of the sodium content (same color legend as in A). The effect of temperature on the EC of the Ciomadul dacite is shown by the thin curves labeled 700 and 900°C. (For interpretation of the colours in the figure, the reader is referred to the web version of this article.)

pre-eruptive and long-storage conditions produce similar electrical signatures. The water content (6.0–7.7 wt.%) deduced for the low-temperature crystal mush is relatively close to the water saturation pressure of dacitic melts (Proureau and Scaillet, 2003) at the depth of the geophysical anomaly; this is consistent and plausible in the case of a mushy magma that partially crystallized and concentrated the water in the melt. Our melt fraction estimations would be underestimated if  $\text{CO}_2$  were present, because  $\text{CO}_2$  decreases the amount of water in the volatile phase, and thus indirectly the electrical conductivity (Iacono-Marziano et al., 2012; Ni et al., 2011).

If the residual liquid had, however, a rhyolitic rather than a dacitic composition, as deduced from glasses in felsic crystal clots and glass inclusions hosted by minerals equilibrated at relatively shallow conditions (715°C), then, it would impact on the estimation of the melt fraction using electrical conductivity. These glasses have a peraluminous composition determined from the aluminum saturation index (Appendix B), which is similar to the rhyolitic melts that were electrically characterized by Chen et al. (Chen et al., 2018). Under similar conditions (400 MPa, 7.0 wt.%  $\text{H}_2\text{O}$ ), the peraluminous rhyolite is as conductive as the dacite and the per-

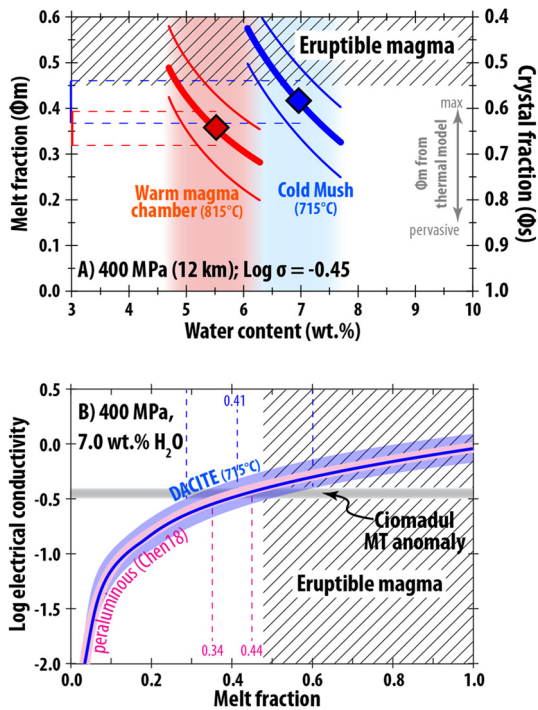


**Fig. 9.** Melt fraction beneath Ciomadul volcano. (A) The melt fraction and water content respecting the electrical anomaly ( $\text{Log } \sigma = -0.45$ ) observed by magnetotelluric survey (Harangi et al., 2015b) for both reservoir and mush cases. The curves are truncated according to the possible range of water content constrained by the petrology of the Ciomadul dacite, providing the likely range of melt fraction in the upper crust reservoir. Diamond symbols show the “preferred values” presented in Table 2. The “eruptible magma” field corresponds to melt fraction higher than 0.45 resulting in remobilisable magma (Cooper and Kent, 2014). (B) Electrical conductivity vs. melt fraction of the Ciomadul dacite and a peraluminous rhyolite (Chen et al., 2018) similar to the glass observed in Ciomadul felsic crystal clots.

vative melt fraction would be the same (0.34 to 0.44) to explain the geophysical anomaly ( $\text{Log } \sigma = -0.4$  to  $-0.5$ ; Fig. 9B).

Melt fractions deduced from numerical simulations are lower than the values determined from electrical conductivity measurements: the calculated average melt fraction (0.14) of the magma body corresponds to electrical conductivities about  $\text{Log } -0.6$ . Such average melt fraction pervasively distributed cannot explain the current electrical anomaly (Harangi et al., 2015b). However, the heterogeneous melt distribution predicted by the numerical model (Fig. 5C) with regions with higher melt fraction (up to 0.40) distributed in the magma body is a plausible explanation for the electrical anomaly as deduced experimentally. Whatever the configuration, both numerical and experimental approaches consistently show that a reservoir with significant content of hydrous melt could still exist beneath Ciomadul volcano, despite its long dormancy and its moderate reservoir size.

#### 4.4. Extinct, long-dormant and potentially active volcanoes

By combining petrologic observations, geophysical results, experimental conductivity data of its last volcanic products and thermal modelling for the development of its magma storage, we are able to decipher the present-day nature of the subvolcanic magmatic plumbing system beneath the long-dormant Ciomadul volcano. Although it is generally considered as extinct (last eruption is ca. 30 ka), the significant average melt fraction determined in the upper crustal magma storage makes the volcano still potentially active. This conclusion is supported also by  $\text{CO}_2$  degassing (over 10,000 tonnes/year emission flux) with isotopic composition implying a strong magmatic component (Kis et al., 2019). Based on

magnetotelluric reconstruction (Harangi et al., 2015b) of the current upper crustal magma reservoir, the thermal evolution of the system and experimental constraints from electrical conductivity measurements, the total volume of the upper crustal melt-bearing mush beneath Ciomadul nowadays could be of the order of 100  $\text{km}^3$ , with a melt volume from  $\sim 15$  up to 58  $\text{km}^3$  based on numerical and experimental determinations. Such volume exceeds the estimated volume of magma involved during the development of the entire volcanic complex (Szakács et al., 2015) (8–14  $\text{km}^3$ ), meaning that most of magma transferred to the upper crust has not erupted. The likely persistence of melt and the existence of local high melt fractions within a relatively cold mush support the theory of magma storage for prolonged ( $>10$ 's kyr) periods above the solidus (Szymanowski et al., 2017). Such condition could characterize not only the active and potentially active volcanoes, but also other seemingly inactive volcanoes, worldwide.

Although (1) a volcano is generally considered as extinct when its quiescence period exceeds 10 kyr and (2) we cannot predict an upcoming eruption at Ciomadul, we show that determining the state of a volcano and evaluating the associated potential hazard is critical, and must be performed primarily by characterizing the nature of the subvolcanic magma storage condition. Ciomadul is not a unique case; the development of remote observation techniques permits the detection of geophysical anomalies beneath emblematic long-dormant volcanoes. The best example is the Yellowstone, where the last eruption occurred 70 ka, yet it lies above a massive magma reservoir with significant amount of melt (Huang et al., 2015). The Cerro Uturuncu in Bolivia erupted last time 270 ka (Sparks et al., 2008), but recent uplift and seismicity imply an active subvolcanic magma storage, which was detected also by geophysical methods (Comeau et al., 2016). A slow rejuvenation of the magma system beneath Colli Albani in Italy was also proposed (Iacono Marziano et al., 2007), despite its last eruption occurred around 20–36 ka. The presence of significant melt fraction beneath Ciomadul and other long-dormant volcanoes does not imply imminent eruption, but shows that these volcanoes pose a potential and underrated threat to the population unaware of the volcanic risk close by. The term, volcanoes with potential active magma storage (PAMS volcano) could emphasize their importance.

## 5. Conclusions

With a multidisciplinary approach, we characterize the magmatic system of Ciomadul, a seemingly inactive volcano at eastern-central Europe. Petrology and thermobarometry on amphiboles from a 32 ka lava dome dacite (one of the latest eruption products) reveals three main conditions of crystallization: (1) low pressure and temperature ( $\sim 715^\circ\text{C}$ ) corresponding to a mushy upper crust reservoir, (2) relatively warm ( $>900^\circ$ ) and deep conditions that we attribute to the deeper part of the mushy reservoir and (3) intermediate conditions ( $\sim 815^\circ\text{C}$ ) typical of all amphibole rims that we attribute to pre-eruptive conditions at the shallow level. This dominantly felsic upper crustal mushy magma storage is underlain by a hot lower crustal zone with mafic magma accumulation. Such features demonstrate the transcrustal magmatic system beneath Ciomadul and were used to run numerical simulation about its thermal evolution. The simulations predict the slow cooling of the upper reservoir and the persistence of at least 15% of melt (locally reaching up to 40%). We finally tested these predictions by performing experiments on the dacite with in situ electrical conductivity measurements. We find that the geophysical anomaly identified beneath Ciomadul can be explained by an upper crustal magma reservoir, which contains between 20 and 58% of nearly water-saturated dacitic to rhyolitic melt. Such thermal evolution and presence of melt is consistent with a magma storage existing for a protracted time (around 350 kyr; (Harangi et al., 2015a) and

supports the hypothesis of long-lasting, persistent magma storage above the solidus (Szymanowski et al., 2017). From experiments and thermal calculations, we demonstrate here that Ciomadul magmatic system could locally contain significant amount of melt with relative fraction close to the eruptible state in some regions. Such magma storage conditions can exist even beneath relatively small volcanic complexes. As long as melt-bearing magma body can be inferred beneath such long-dormant volcanoes, the potential for rejuvenation exists, irrespective of the length of its quiescence time and this calls for more attention to apparently inactive PAMS volcanoes.

### Acknowledgements

This project was supported by ERC #279790 and ANR #2010 BLANG2101 projects attributed to FG; OTKA-NKFIH K116528 (SH) and NKFIH PD 121048 (RL) research grants from Romanian Government. OK and OB acknowledge the support from SNF Grant #200021\_178928. ML acknowledges the French Government Laboratory of Excellence initiative (ClerVolc contribution number 341). IS benefited by a grant of the Ministry of Research and Innovation, CNCS-UEFISCDI, project PN-III-P4-ID-PCCF-2016-0014, within PNCDI III. We thank C. Miller and M. Petrelli for their reviews that greatly clarified the paper.

### Appendix. Supplementary material

Supplementary material related to this article can be found online at <https://doi.org/10.1016/j.epsl.2019.06.004>.

### References

- Anderson, J.L., Barth, A.P., Wooden, J.L., Mazdab, F., 2008. Thermometers and thermobarometers in granitic systems. *Rev. Mineral. Geochem.* 69, 121–142.
- Annen, C., Blundy, J.D., Sparks, R.S.J., 2006. The genesis of intermediate and silicic magmas in deep crustal hot zones. *J. Petrol.* 47, 505–539. <https://doi.org/10.1093/ptrology/egi084>.
- Bachmann, O., 2010. The petrologic evolution and pre-eruptive conditions of the rhyolitic Kos Plateau Tuff (Aegean arc). *Open Geosci.* 2, 270–305.
- Bachmann, O., Huber, C., 2016. Silicic magma reservoirs in the Earth's crust. *Am. Mineral.* 101, 2377–2404.
- Barboni, M., Boehnke, P., Schmitt, A.K., Harrison, T.M., Shane, P., Bouvier, A.-S., Baumgartner, L., 2016. Warm storage for arc magmas. *Proc. Natl. Acad. Sci.* 113, 13959–13964.
- Bedrosian, P.A., 2007. MT+, integrating magnetotellurics to determine earth structure, physical state, and processes. *Surv. Geophys.* 28, 121–167.
- Carrigan, C.R., 1988. Biot number and thermos bottle effect: implications for magma-chamber convection. *Geology* 16, 771–774.
- Cashman, K.V., Sparks, R.S.J., Blundy, J.D., 2017. Vertically extensive and unstable magmatic systems: a unified view of igneous processes. *Science* 80, 355. eaag3055.
- Chen, J., Gaillard, F., Villaros, A., Yang, X., Laumonier, M., Jolivet, L., Unsworth, M., Hashim, L., Scaillet, B., Richard, G., 2018. Melting conditions in the modern Tibetan crust since the Miocene. *Nat. Commun.* 9. <https://doi.org/10.1038/s41467-018-05934-7>.
- Christopher, T.E., Blundy, J., Cashman, K., Cole, P., Edmonds, M., Smith, P.J., Sparks, R.S.J., Stinton, A., 2015. Crustal-scale degassing due to magma system destabilization and magma-gas decoupling at Soufrière Hills Volcano, Montserrat. *Geochem. Geophys. Geosyst.* 16, 2797–2811.
- Cloetingh, S.A.P.L., Burov, E., Matenco, L., Toussaint, G., Bertotti, G., Andriessen, P.A.M., et al., 2004. Thermo-mechanical controls on the mode of continental collision in the SE Carpathians (Romania). *Earth Planet. Sci. Lett.* 218 (1–2), 57–76.
- Comeau, M.J., Unsworth, M.J., Cordell, D., 2016. New constraints on the magma distribution and composition beneath Volcán Uturuncu and the southern Bolivian Altiplano from magnetotelluric data. *Geosphere* 12, 1391–1421.
- Cooper, K.M., 2019. Time scales and temperatures of crystal storage in magma reservoirs: implications for magma reservoir dynamics. *Philos. Trans. R. Soc. Lond. Ser. A* 377, 20180009.
- Cooper, K.M., 2015. Timescales of crustal magma reservoir processes: insights from U-series crystal ages. *Geol. Soc. (Lond.) Spec. Publ.* 422 SP422-7.
- Cooper, K.M., Kent, A.J., 2014. Rapid remobilization of magmatic crystals kept in cold storage. *Nature* 506 (7489), 480.
- Costa, F., 2008. Residence times of silicic magmas associated with calderas. *Dev. Volcanol.* 10, 1–55.
- Dufek, J., Bachmann, O., 2010. Quantum magmatism: magmatic compositional gaps generated by melt-crystal dynamics. *Geology* 38, 687–690. <https://doi.org/10.1130/G30831.1>.
- Erdmann, S., Martel, C., Pichavant, M., Kushnir, A., 2014. Amphibole as an archivist of magmatic crystallization conditions: problems, potential, and implications for inferring magma storage prior to the paroxysmal 2010 eruption of Mount Merapi, Indonesia. *Contrib. Mineral. Petrol.* 167, 1016.
- Féménias, O., Mercier, J.-C.C., Nkono, C., Diot, H., Berza, T., Tatu, M., Demaiffe, D., 2006. Calcic amphibole growth and compositions in calc-alkaline magmas: evidence from the Motru Dike Swarm (Southern Carpathians, Romania). *Am. Mineral.* 91, 73–81.
- Ferry, J.M., Watson, E.B., 2007. New thermodynamic models and revised calibrations for the Ti-in-zircon and Zr-in-rutile thermometers. *Contrib. Mineral. Petrol.* 154, 429–437.
- Gaillard, F., 2004. Laboratory measurements of electrical conductivity of hydrous and dry silicic melts under pressure. *Earth Planet. Sci. Lett.* 218, 215–228.
- Gaillard, F., Marziano, G.L., 2005. Electrical conductivity of magma in the course of crystallization controlled by their residual liquid composition. *J. Geophys. Res., Solid Earth* 110.
- Gelman, S.E., Gutiérrez, F.J., Bachmann, O., 2013. On the longevity of large upper crustal silicic magma reservoirs. *Geology* 41, 759–762.
- Glover, P.W.J., Hole, M.J., Pous, J., 2000. A modified Archie's law for two conducting phases. *Earth Planet. Sci. Lett.* 180, 369–383.
- Gorini, A., Ridolfi, F., Piscaglia, F., Taussi, M., Renzulli, A., 2018. Application and reliability of calcic amphibole thermobarometry as inferred from calc-alkaline products of active geothermal areas in the Andes. *J. Volcanol. Geotherm. Res.* 358, 58–76.
- Gualda, G.A.R., Ghiorso, M.S., Lemons, R.V., Carley, T.L., 2012. Rhyolite-MELTS: a modified calibration of MELTS optimized for silica-rich, fluid-bearing magmatic systems. *J. Petrol.* 53, 875–890.
- Guo, X., Zhang, L., Behrens, H., Ni, H., 2016. Probing the status of felsic magma reservoirs: Constraints from the P–T–H<sub>2</sub>O dependences of electrical conductivity of rhyolitic melt. *Earth Planet. Sci. Lett.* 433, 54–62.
- Harangi, S., Lenkey, L., 2007. Genesis of the Neogene to Quaternary volcanism in the Carpathian-Pannonian region: role of subduction, extension, and mantle plume. *Spec. Pap., Geol. Soc. Am.* 418, 67.
- Harangi, S., Lukács, R., Schmitt, A.K., Dunkl, I., Molnár, K., Kiss, B., Seghedi, I., Novothny, Á., Molnár, M., 2015a. Constraints on the timing of Quaternary volcanism and duration of magma residence at Ciomadul volcano, east-central Europe, from combined U–Th/He and U–Th zircon geochronology. *J. Volcanol. Geotherm. Res.* 301, 66–80.
- Harangi, S., Molnár, M., Vinkler, A.P., Kiss, B., Jull, A.J.T., Leonard, A.G., 2010. Radiocarbon dating of the last volcanic eruptions of Ciomadul volcano, Southeast Carpathians, eastern-central Europe. *Radiocarbon* 52, 1498–1507.
- Harangi, S., Novák, A., Kiss, B., Seghedi, I., Lukács, R., Szarka, L., Wesztergom, V., Metwally, M., Gribovszki, K., 2015b. Combined magnetotelluric and petrologic constraints for the nature of the magma storage system beneath the Late Pleistocene Ciomadul volcano (SE Carpathians). *J. Volcanol. Geotherm. Res.* 290, 82–96.
- Hashim, L., Gaillard, F., Champallier, R., Le Breton, N., Arbaret, L., Scaillet, B., 2013. Experimental assessment of the relationships between electrical resistivity, crustal melting and strain localization beneath the Himalayan–Tibetan Belt. *Earth Planet. Sci. Lett.* 373, 20–30.
- Hauser, F., Raileanu, V., Fielitz, W., Dinu, C., 2007. Seismic crustal structure between the Transylvanian Basin and the Black Sea, Romania. *Tectonophysics* 430, 1–25. <https://doi.org/10.1016/j.tecto.2006.10.005>.
- Hildreth, W., Moorbath, S., 1988. Crustal contributions to arc magmatism in the Andes of central Chile. *Contrib. Mineral. Petrol.* 98, 455–489.
- Holland, T., Blundy, J., 1994. Non-ideal interactions in calcic amphiboles and their bearing on amphibole-plagioclase thermometry. *Contrib. Mineral. Petrol.* 116, 433–447.
- Huber, C., Bachmann, O., Manga, M., 2009. Homogenization processes in silicic magma chambers by stirring and mushification (latent heat buffering). *Earth Planet. Sci. Lett.* 283, 38–47.
- Huber, C., Bachmann, O., Dufek, J., 2011. Thermo-mechanical reactivation of locked crystal mushes: melting-induced internal fracturing and assimilation processes in magmas. *Earth Planet. Sci. Lett.* 304, 443–454.
- Huang, H.-H., Lin, F.-C., Schmandt, B., Farrell, J., Smith, R.B., Tsai, V.C., 2015. The Yellowstone magmatic system from the mantle plume to the upper crust. *Science* 80 (348), 773–776.
- Iacono Marziano, G., Gaillard, F., Pichavant, M., 2007. Limestone assimilation and the origin of CO<sub>2</sub> emissions at the Alban Hills (Central Italy): constraints from experimental petrology. *J. Volcanol. Geotherm. Res.* 166, 91–105. <https://doi.org/10.1016/j.jvolgeores.2007.07.001>.
- Iacono-Marziano, G., Morizet, Y., Le Trong, E., Gaillard, F., 2012. New experimental data and semi-empirical parameterization of H<sub>2</sub>O–CO<sub>2</sub> solubility in mafic melts. *Geochim. Cosmochim. Acta* 97, 1–23. <https://doi.org/10.1016/j.gca.2012.08.035>.
- Ismail-Zadeh, A., Matenco, L., Radulian, M., Cloetingh, S., Panza, G., 2012. Geodynamics and intermediate-depth seismicity in Vrancea (the south-eastern Carpathians): current state-of-the art. *Tectonophysics* 530, 50–79.
- Karakas, O., Degruyter, W., Bachmann, O., Dufek, J., 2017. Lifetime and size of shallow magma bodies controlled by crustal-scale magmatism. *Nat. Geosci.* 10, 446.



- Karakas, O., Dufek, J., 2015. Melt evolution and residence in extending crust: thermal modeling of the crust and crustal magmas. *Earth Planet. Sci. Lett.* 425, 131–144.
- Karátson, D., Wulf, S., Veres, D., Magyari, E.K., Gertisser, R., Timar-Gabor, A., Novothny, Á., Telbisz, T., Szalai, Z., Anechitei-Deacu, V., 2016. The latest explosive eruptions of Ciomadul (Csomád) volcano, East Carpathians—a tephrostratigraphic approach for the 51–29 ka BP time interval. *J. Volcanol. Geotherm. Res.* 319, 29–51.
- Kis, B.M., Caracausi, A., Palcsu, L., Baciú, C., Ionescu, A., Futó, I., Sciarra, A., Harangi, S., 2019. Noble gas and carbon isotope systematics at the seemingly inactive Ciomadul volcano (Eastern-Central Europe, Romania): evidence for volcanic degassing. *Geochem. Geophys. Geosyst.*
- Kiss, B., Harangi, S., Ntaflós, T., Mason, P.R.D., Pál-Molnár, E., 2014. Amphibole perspective to unravel pre-eruptive processes and conditions in volcanic plumbing systems beneath intermediate arc volcanoes: a case study from Ciomadul volcano (SE Carpathians). *Contrib. Mineral. Petrol.* 167, 986.
- Laumonier, M., Farla, R., Frost, D.J., Katsura, T., Marquardt, K., Bouvier, A.S., Baumgartner, L.P., 2017a. Experimental determination of melt interconnectivity and electrical conductivity in the upper mantle. *Earth Planet. Sci. Lett.* 463, 286–297. <https://doi.org/10.1016/j.epsl.2017.01.037>.
- Laumonier, M., Gaillard, F., Muir, D., Blundy, J., Unsworth, M., 2017b. Giant magmatic water reservoirs at mid-crustal depth inferred from electrical conductivity and the growth of the continental crust. *Earth Planet. Sci. Lett.* 457, 173–180. <https://doi.org/10.1016/j.epsl.2016.10.023>.
- Laumonier, M., Gaillard, F., Sifré, D., 2015. The effect of pressure and water concentration on the electrical conductivity of dacitic melts: implication for magnetotelluric imaging in subduction areas. *Chem. Geol.* 418, 66–76.
- Martin, M., Wenzel, F., CALIXTO Working Group, 2006. High-resolution teleseismic body wave tomography beneath SE-Romania-II. Imaging of a slab detachment scenario. *Geophys. J. Int.* 164 (3), 579–595.
- Maury, R., 1968. Conductibilité électrique des tectosilicates. II. Discussion des résultats. *Bull. Soc. Fr. Minéral. Cristallogr.* 91, 355–366.
- Molnár, K., Harangi, S., Lukács, R., Dunkl, I., Schmitt, A.K., Kiss, B., Garamhegyi, T., Seghedi, I., 2018. The onset of the volcanism in the Ciomadul Volcanic Dome Complex (Eastern Carpathians): eruption chronology and magma type variation. *J. Volcanol. Geotherm. Res.* 354, 39–56.
- Molnár, K., Lukács, R., Dunkl, I., Schmitt, A.K., Kiss, B., Seghedi, I., Szepesi, J., Harangi, S., 2019. Episodes of dormancy and eruption of the Late Pleistocene Ciomadul volcanic complex (Eastern Carpathians, Romania) constrained by zircon geochronology. *J. Volcanol. Geotherm. Res.* 373, 133–147. <https://doi.org/10.1016/j.jvolgeores.2019.01.025>.
- Mutch, E.J.F., Blundy, J.D., Tattitch, B.C., Cooper, F.J., Brooker, R.A., 2016. An experimental study of amphibole stability in low-pressure granitic magmas and a revised Al-in-hornblende geobarometer. *Contrib. Mineral. Petrol.* 171, 85.
- Nandedkar, R.H., Ulmer, P., Müntener, O., 2014. Fractional crystallization of primitive, hydrous arc magmas: an experimental study at 0.7 GPa. *Contrib. Mineral. Petrol.* 167, 1015.
- Ni, H., Keppler, H., Behrens, H., 2011. Electrical conductivity of hydrous basaltic melts: implications for partial melting in the upper mantle. *Contrib. Mineral. Petrol.* 162, 637–650. <https://doi.org/10.1007/s00410-011-0617-4>.
- Ohlhorst, S., Behrens, H., Holtz, F., 2001. Compositional dependence of molar absorptivities of near-infrared OH- and H<sub>2</sub>O bands in rhyolitic to basaltic glasses. *Chem. Geol.* 174, 5–20.
- Patankar, S. *Numerical Heat Transfer and Fluid Flow*. CRC Press, 1980.
- Petrelli, M., El Omari, K., Spina, L., Le Guer, Y., La Spina, G., Perugini, D., 2018. Timescales of water accumulation in magmas and implications for short warning times of explosive eruptions. *Nat. Commun.* 9, 770.
- Pommier, A., Gaillard, F., Pichavant, M., Scaillet, B., 2008. Laboratory measurements of electrical conductivities of hydrous and dry Mount Vesuvius melts under pressure. *J. Geophys. Res., Solid Earth* 113.
- Popa, M., Radulian, M., Szakács, A., Seghedi, I., Zaharia, B., 2012. New seismic and tomography data in the southern part of the Harghita Mountains (Romania, Southeastern Carpathians): connection with recent volcanic activity. *Pure Appl. Geophys.* 169, 1557–1573.
- Prouteau, G., Scaillet, B., 2003. Experimental constraints on the origin of the 1991 Pinatubo dacite. *J. Petrol.* 44, 2203–2241.
- Ridolfi, F., Renzulli, A., 2012. Calcic amphiboles in calc-alkaline and alkaline magmas: thermobarometric and chemometric empirical equations valid up to 1,130°C and 2.2 GPa. *Contrib. Mineral. Petrol.* 163, 877–895.
- Ridolfi, F., Renzulli, A., Puerini, M., 2010. Stability and chemical equilibrium of amphibole in calc-alkaline magmas: an overview, new thermobarometric formulations and application to subduction-related volcanoes. *Contrib. Mineral. Petrol.* 160, 45–66.
- Rubin, A.E., Cooper, K.M., Till, C.B., Kent, A.J.R., Costa, F., Bose, M., Gravley, D., Deering, C., Cole, J., 2017. Rapid cooling and cold storage in a silicic magma reservoir recorded in individual crystals. *Science* 80 (356), 1154–1156.
- Seghedi, I., Downes, H., 2011. Geochemistry and tectonic development of Cenozoic magmatism in the Carpathian–Pannonian region. *Gondwana Res.* 20, 655–672.
- Sifré, D., Gardés, E., Massuyeau, M., Hashim, L., Hier-Majumder, S., Gaillard, F., 2014. Electrical conductivity during incipient melting in the oceanic low-velocity zone. *Nature* 508, 81–85. <https://doi.org/10.1038/nature13245>.
- Sparks, R.S.J., Folkes, C.B., Humphreys, M.C.S., Barfod, D.N., Clavero, J., Sunagua, M.C., McNutt, S.R., Pritchard, M.E., 2008. Uturuncu volcano, Bolivia: volcanic unrest due to mid-crustal magma intrusion. *Am. J. Sci.* 308, 727–769.
- Szakács, A., 1994. Redefining active volcanoes: a discussion. *Bull. Volcanol.* 56, 321–325.
- Szakács, A., Seghedi, I., Pécskay, Z., Mirea, V., 2015. Eruptive history of a low-frequency and low-output rate Pleistocene volcano, Ciomadul, South Harghita Mts. *Bull. Volcanol.* 77 (12).
- Szymanowski, D., Wotzlaw, J.F., Ellis, B.S., Bachmann, O., Guillong, M., Von Quadt, A., 2017. Protracted near-solidus storage and pre-eruptive rejuvenation of large magma reservoirs. *Nat. Geosci.* 10, 777–782. <https://doi.org/10.1038/ngeo3020>.
- Tyburczy, J.A., Waff, H.S., 1985. High pressure electrical conductivity in naturally occurring silicate liquids. *Point Defects Miner.* 31, 78–87.
- Vielzeuf, D., Holloway, J.R., 1988. Experimental determination of the fluid-absent melting relations in the pelitic system. *Contrib. Mineral. Petrol.* 98, 257–276.
- Vinkler, A.P., Harangi, S., Ntaflós, T., Szakács, A., 2007. A Csomád vulkán (Keleti-Kárpátok) horzszaköveinek kőzettani és geokémiai vizsgálata—petrogenetikai következtetések (Petrology and geochemistry of the pumices from the Ciomadul volcano [Eastern Carpathians]—implications for the petrogenetic processes). *Földt. Közöny* 137, 103–128.
- Voller, V.R., Swaminathan, C.R., 1991. ERAL source-based method for solidification phase change. *Numer. Heat Transf., Part B, Fundam.* 19, 175–189.
- Waters, L.E., Lange, R.A., 2015. An updated calibration of the plagioclase-liquid hygrometer-thermometer applicable to basalts through rhyolites. *Am. Mineral.* 100, 2172–2184.
- Watson, E.B., Wark, D.A., Thomas, J.B., 2006. Crystallization thermometers for zircon and rutile. *Contrib. Mineral. Petrol.* 151, 413.